

## Templated fabrication of large area subwavelength antireflection gratings on silicon

Chih-Hung Sun, Wei-Lun Min, Nicholas C. Linn, and Peng Jiang<sup>a)</sup>

*Department of Chemical Engineering, University of Florida, Gainesville, Florida 32611, USA*

Bin Jiang

*Department of Mathematics and Statistics, Portland State University, Portland, Oregon 97201, USA*

(Received 2 October 2007; accepted 15 November 2007; published online 5 December 2007)

We report a cheap and scalable bottom-up technique for fabricating wafer-scale, subwavelength-structured antireflection coatings on single-crystalline silicon substrates. Spin-coated monolayer colloidal crystals are utilized as shadow masks to generate metallic nanohole arrays. Inverted pyramid arrays in silicon can then be templated against nanoholes by anisotropic wet etching. The resulting subwavelength gratings greatly suppress specular reflection at normal incidence. The reflection spectra for flat silicon and the templated gratings at long wavelengths agree well with the simulated results using a rigorous coupled wave analysis model. These subwavelength gratings are of great technological importance in crystalline silicon solar cells. © 2007 American Institute of Physics. [DOI: 10.1063/1.2821833]

Current production of solar cells is dominated by crystalline silicon modules;<sup>1,2</sup> however, due to the high refractive index of silicon, more than 30% of incident light is reflected back, which greatly reduces the conversion efficiency of photovoltaic devices.<sup>3-5</sup> To significantly suppress the reflective loss of solar cells, various antireflection techniques, such as quarter-wavelength multilayer films and nanoporous coatings, have been developed.<sup>3,6-16</sup> For crystalline silicon solar cells, silicon nitride films deposited by plasma enhanced chemical vapor deposition have become the industry standard for antireflection coatings (ARCs).<sup>3</sup> Unfortunately, these existing techniques often perform suboptimally or are expensive to implement, impeding development of solar cells that can be made truly economically competitive with fossil fuels.

Inspired by the microstructured cornea of some nocturnal moths,<sup>17,18</sup> subwavelength-structured gratings directly patterned on silicon substrates have been extensively explored both experimentally<sup>7,19-28</sup> and theoretically<sup>29-32</sup> for developing broadband ARCs. These gratings with a period smaller than the wavelength of incident light are intrinsically more stable and durable than multilayer ARCs since no foreign material is involved. Electron-beam lithography (EBL) is a common approach in fabricating subwavelength gratings.<sup>22,23</sup> Unfortunately, the low throughput and the high cost of EBL raise big concerns. Interference lithography<sup>7,19</sup> and nanoimprint lithography<sup>28</sup> enable the creation of subwavelength antireflection structures over large areas; however, these techniques are still expensive to implement.

Here, we demonstrate a much simpler and cheaper self-assembly technology in creating wafer-scale subwavelength antireflection gratings on single-crystalline silicon substrates. Contrary to most bottom-up approaches,<sup>21,27</sup> which are favorable for low-volume, laboratory-scale production, this nonlithographic technique is compatible with standard microfabrication, enabling large-scale production of subwavelength ARCs for solar collectors. The technology is based on

the robust spin-coating technological platform we have recently developed for scalable production of periodic nanostructured materials.<sup>33-38</sup>

A schematic illustration of the fabrication procedures for making wafer-scale subwavelength inverted pyramid gratings on single-crystalline silicon wafers is shown in Fig. 1. We start to generate nonclose-packed colloidal monolayers on a (100) silicon wafer (test grade, *n* type, Montco Silicon Technologies) by the spin-coating technology.<sup>33,34</sup> The nonclose-packed silica particles function as shadow masks during an electron-beam evaporation process for depositing a 30 nm thick chromium layer. After lifting off the templating silica particles, a periodic array of nanoholes whose diameter is determined by the size of templating silica spheres can be formed.<sup>36</sup> These circular nanoholes can then be used as etching masks during a KOH anisotropic etching process to create wafer-scale inverted pyramid arrays in silicon substrates.<sup>37</sup>

We are able to control the pyramid size by simply adjusting the anisotropic etching conditions. Figure 2 shows

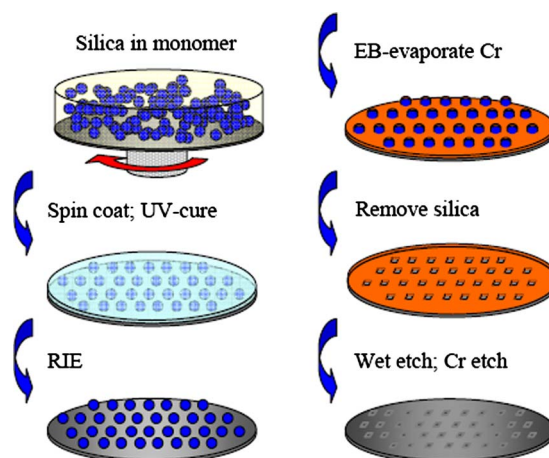


FIG. 1. (Color online) Schematic illustration of the templating procedures for fabricating subwavelength-structured antireflection pyramid gratings on single-crystalline silicon.

<sup>a)</sup>Electronic mail: pjiang@che.ufl.edu

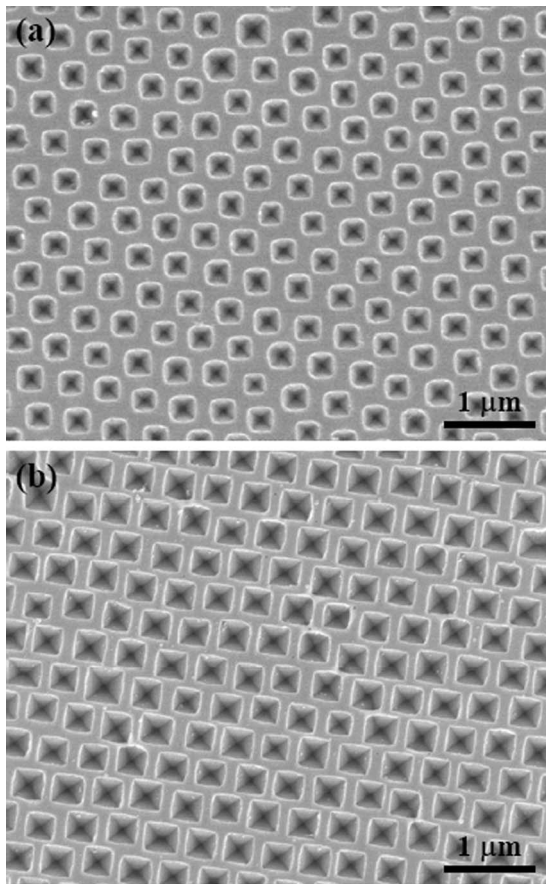


FIG. 2. Replicated inverted pyramid arrays in silicon. (a) The 300 nm size pyramids etched at 60 °C for 90 s. (b) The 360 nm size pyramids etched at 60 °C for 210 s. The 320 nm diameter silica spheres are used as templates.

scanning electron microscope (SEM) images of two inverted pyramid arrays templated from the same spin-coated silica monolayer sample (320 nm particle diameter). The samples are etched in the same solution containing 62.5 g KOH, 50 ml anhydrous 2-propanol, and 200 ml ultrapure water at 60 °C for 90 and 210 s, respectively. It is apparent that longer etching leads to larger pyramids with well-defined square bases, while the less etched samples have rounded corners. The size of the pyramids can be larger than that of the templating silica spheres due to the undercutting of silicon substrates underneath chromium nanoholes. The long-range hexagonal ordering of the templated pyramidal pits is evident from the SEM images. The orthogonal crosses at the centers of the pits confirm the inverted pyramidal structures.<sup>39</sup>

The specular optical reflectivity of the replicated pyramid arrays is evaluated using visible-near-IR reflectivity measurement at normal incidence.<sup>35</sup> The solid lines in Fig. 3 show the measured normal-incidence specular reflection from a polished (100) silicon wafer and the sample, shown in Fig. 2(b), with 360 nm pyramidal pits. The flat silicon substrate exhibits high reflection (>35%) for visible and near-infrared wavelengths, while the subwavelength-structured gratings show reduced reflection of ~10% for long wavelengths (>600 nm). The reflection is further reduced to ~2% for wavelengths around 400 nm. For smaller pyramids, the reflection progressively increases with decreased pyramidal pits.

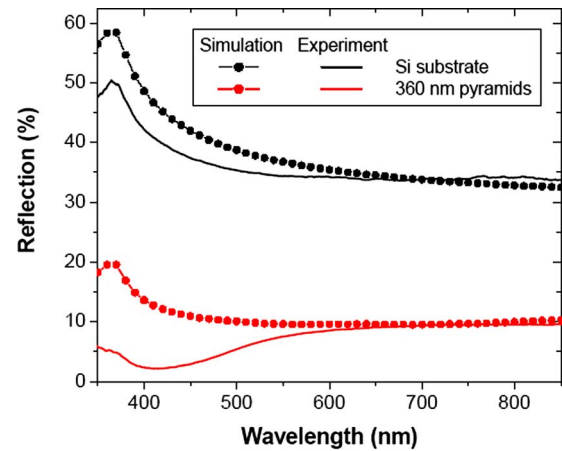


FIG. 3. (Color online) Experimental (solid) and RCWA-modeled (dotted) specular optical reflectivity at normal incidence. Black: bare (100) silicon wafer. Red: 360 nm size pyramids templated from 320 nm silica spheres.

The templated silicon subwavelength gratings exhibit lower reflection than colloid-based antireflection coatings on crystalline silicon solar cells.<sup>5</sup> Though the normal-incidence reflection from the templated pyramid gratings is higher than other subwavelength-structured ARCs made by lithographic techniques with typical reflection of ~2%–10%,<sup>7,19,22,23,28</sup> the cost benefit of this nonlithographic methodology is a major advantage. Additionally, optimization of the templated structures will facilitate further improvement of the antireflection performance. The state-of-the-art silicon nitride ARCs on crystalline silicon solar cells exhibit minimal (<2%) reflection around 600 nm, but the reflection increases to more than 10% for near-IR (>800 nm) and visible (<500 nm) wavelengths, which account for a significant portion of the solar spectrum.<sup>3,5</sup> By contrast, the templated pyramid arrays show relatively low reflection at short wavelengths (Fig. 3).

A multilayer rigorous coupled wave analysis (RCWA) model<sup>40–42</sup> has also been developed to complement the optical measurement. Firstly, we divide the inverted pyramid array into 100 horizontal layers with equal thickness. Since the KOH-etched silicon pyramids have characteristic of 54.7°

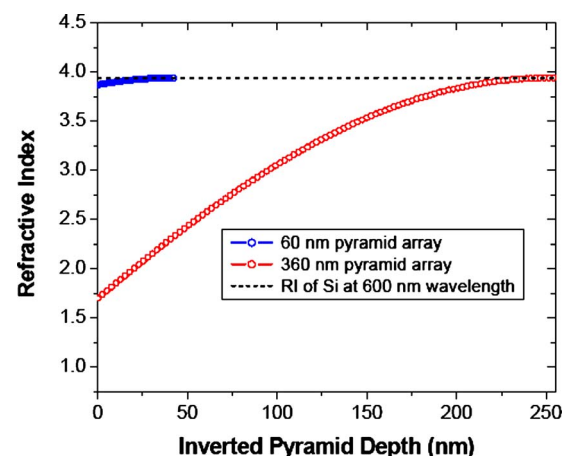


FIG. 4. (Color online) Comparison of the change of calculated effective refractive index at  $\lambda=600$  nm from the wafer surface (depth=0) to the vertex plane of inverted pyramids between a 360 nm pyramid array (red circles) and a 60 nm pyramid array (blue circles). The diameter of templating silica spheres is 320 nm.

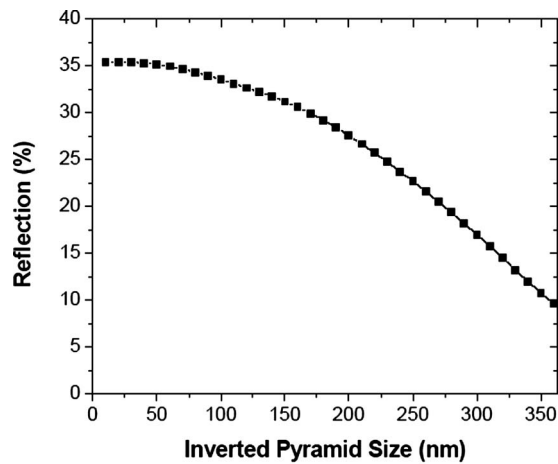


FIG. 5. RCWA-simulated normal-incidence optical reflection at  $\lambda = 600$  nm vs inverted pyramid size. The 320 nm silica spheres are used as templates.

sidewalls, the depth of the anisotropic V-shape pitches is determined by the base length of the pits. Based on the effective medium theory,<sup>43</sup> the effective refractive index  $n(z^*)$  of the layer at level  $z^*$  can be approximated by  $n(z^*) = [f(z^*)\tilde{N}_{\text{Si}}^q + [1 - f(z^*)]n_{\text{air}}^q]^{1/q}$ , where  $f(z^*)$  is the fraction of silicon contained in the layer,  $\tilde{N}_{\text{Si}} = n + ik$  is the complex refractive index of silicon ( $n$  and  $k$  are optical constants),  $n_{\text{air}} = 1$ , and  $q = \frac{2}{3}$ .<sup>43</sup> The optical constants of silicon which are functions of wavelengths are obtained from literature.<sup>44</sup> Secondly, we calculate the reflectance of the whole system by solving the Maxwell equation to express the electromagnetic (EM) field in each layer and then match EM boundary conditions between neighboring layers for the determination of the reflectance of the system.

The RCWA-simulated reflection for a bare silicon substrate and an inverted pyramid array in silicon with 360 nm base length are shown by the dotted lines in Fig. 3. It is apparent that the theoretical prediction for single-crystalline silicon is close to the experimental spectrum, while for the subwavelength-structured pyramid gratings, the modeling results only match with experimental data when the wavelength is large. The difference tends to be large when the wavelength becomes small. This is due to the limitation of the modeling where each layer is assumed to have a uniform refractive index,<sup>42</sup> which is, in fact, a two-dimensional periodic function at each layer. Meanwhile, the effective refractive index formula is only accurate when the wavelength of light is larger than the period of the pyramid arrays.<sup>43</sup>

To understand the improved antireflection performance for subwavelength-structured pyramid arrays, we plot the calculated real part of the complex refractive index at  $\lambda = 600$  nm versus the depth of pyramids with 60 nm (blue circles) and 360 nm (red circles) base lengths in Fig. 4. For 60 nm size pyramids, the refractive index changes sharply at the interface between air and the structured silicon surface. The graded index, which is desirable for suppressing the optical reflection,<sup>18</sup> is observed for 360 nm pyramids—the refractive index changes from 1.0 to  $\sim 1.7$  at the air/silicon interface and then gradually changes to the bulk index of silicon. We further calculate the normal-incidence reflection at  $\lambda = 600$  nm for pyramid array samples with different sizes and the results are shown in Fig. 5. It is apparent that larger

pyramids lead to lower reflection, matching our experimental observation.

In summary, we have developed a cheap and scalable nonlithographic approach for creating subwavelength-structured antireflection coatings directly on single-crystalline silicon substrates.

This work was supported in part by the NSF under Grant No. CBET-0651780, the start-up funds from the University of Florida, and the UF Research Incentive Seed Fund.

<sup>1</sup>US Department of Energy Report of the Basic Energy Sciences Workshop on Solar Energy Utilization, 18–21 April 2005 (unpublished).

<sup>2</sup>*Handbook of Photovoltaic Science and Engineering*, edited by A. Luque and S. Hegedus (Wiley, West Sussex, 2003), p. 268.

<sup>3</sup>P. Doshi, G. E. Jellison, and A. Rohatgi, *Appl. Opt.* **36**, 7826 (1997).

<sup>4</sup>A. Gombert, W. Glaubitt, K. Rose, J. Dreiholz, B. Blasi, A. Heinzl, D. Sporn, W. Doll, and V. Wittwer, *Thin Solid Films* **351**, 73 (1999).

<sup>5</sup>B. G. Prevo, E. W. Hon, and O. D. Velev, *J. Mater. Chem.* **17**, 791 (2007).

<sup>6</sup>D. G. Chen, *Sol. Energy Mater. Sol. Cells* **68**, 313 (2001).

<sup>7</sup>P. Lalanne and G. M. Morris, *Nanotechnology* **8**, 53 (1997).

<sup>8</sup>S. Chattopadhyay, L. C. Chen, and K. H. Chen, *Crit. Rev. Solid State Mater. Sci.* **31**, 15 (2006).

<sup>9</sup>P. T. Hammond, *Adv. Mater. (Weinheim, Ger.)* **16**, 1271 (2004).

<sup>10</sup>J. Hiller, J. D. Mendelsohn, and M. F. Rubner, *Nat. Mater.* **1**, 59 (2002).

<sup>11</sup>M. Ibn-Elhaj and M. Schadt, *Nature (London)* **410**, 796 (2001).

<sup>12</sup>H. Y. Koo, D. K. Yi, S. J. Yoo, and D. Y. Kim, *Adv. Mater. (Weinheim, Ger.)* **16**, 274 (2004).

<sup>13</sup>B. G. Prevo, Y. Hwang, and O. D. Velev, *Chem. Mater.* **17**, 3642 (2005).

<sup>14</sup>S. Walheim, E. Schaffer, J. Mlynek, and U. Steiner, *Science* **283**, 520 (1999).

<sup>15</sup>Z. Z. Wu, J. Walish, A. Nolte, L. Zhai, R. E. Cohen, and M. F. Rubner, *Adv. Mater. (Weinheim, Ger.)* **18**, 2699 (2006).

<sup>16</sup>J. Q. Xi, M. F. Schubert, J. K. Kim, E. F. Schubert, M. F. Chen, S. Y. Lin, W. Liu, and J. A. Smart, *Nat. Photonics* **1**, 176 (2007).

<sup>17</sup>P. B. Clapham and M. C. Hutley, *Nature (London)* **244**, 281 (1973).

<sup>18</sup>D. G. Stavenga, S. Foletti, G. Palasantzas, and K. Arikawa, *Proc. R. Soc. London, Ser. B* **273**, 661 (2006).

<sup>19</sup>C. Aydin, A. Zaslavsky, G. J. Sonek, and J. Goldstein, *Appl. Phys. Lett.* **80**, 2242 (2002).

<sup>20</sup>C. Heine and R. H. Morf, *Appl. Opt.* **34**, 2476 (1995).

<sup>21</sup>Y. Kanamori, K. Hane, H. Sai, and H. Yugami, *Appl. Phys. Lett.* **78**, 142 (2001).

<sup>22</sup>Y. Kanamori, E. Roy, and Y. Chen, *Microelectron. Eng.* **78-79**, 287 (2005).

<sup>23</sup>Y. Kanamori, M. Sasaki, and K. Hane, *Opt. Lett.* **24**, 1422 (1999).

<sup>24</sup>F. Nikolajeff, B. Lofving, M. Johansson, J. Bengtsson, S. Hard, and C. Heine, *Appl. Opt.* **39**, 4842 (2000).

<sup>25</sup>C. C. Striener and P. M. Fauchet, *Appl. Phys. Lett.* **81**, 2980 (2002).

<sup>26</sup>S. Wang, X. Z. Yu, and H. T. Fan, *Appl. Phys. Lett.* **91**, 061105 (2007).

<sup>27</sup>C. T. Wu, F. H. Ko, and C. H. Lin, *Appl. Phys. Lett.* **90**, 171911 (2007).

<sup>28</sup>Z. N. Yu, H. Gao, W. Wu, H. X. Ge, and S. Y. Chou, *J. Vac. Sci. Technol. B* **21**, 2874 (2003).

<sup>29</sup>E. B. Grann, M. G. Moharam, and D. A. Pommet, *J. Opt. Soc. Am. A* **12**, 333 (1995).

<sup>30</sup>W. H. Southwell, *J. Opt. Soc. Am. A* **8**, 549 (1991).

<sup>31</sup>B. S. Thornton, *J. Opt. Soc. Am.* **65**, 267 (1975).

<sup>32</sup>J. Zhao and M. A. Green, *IEEE Trans. Electron Devices* **38**, 1925 (1991).

<sup>33</sup>P. Jiang and M. J. McFarland, *J. Am. Chem. Soc.* **126**, 13778 (2004).

<sup>34</sup>P. Jiang, T. Prasad, M. J. McFarland, and V. L. Colvin, *Appl. Phys. Lett.* **89**, 011908 (2006).

<sup>35</sup>N. C. Linn, C. H. Sun, P. Jiang, and B. Jiang, *Appl. Phys. Lett.* **91**, 101108 (2007).

<sup>36</sup>P. Jiang and M. J. McFarland, *J. Am. Chem. Soc.* **127**, 3710 (2005).

<sup>37</sup>C. H. Sun, N. C. Linn, and P. Jiang, *Chem. Mater.* **19**, 4551 (2007).

<sup>38</sup>P. Jiang, *Langmuir* **22**, 3955 (2006).

<sup>39</sup>J. Henzie, E. S. Kwak, and T. W. Odom, *Nano Lett.* **5**, 1199 (2005).

<sup>40</sup>M. G. Moharam and T. K. Gaylord, *J. Opt. Soc. Am.* **71**, 811 (1981).

<sup>41</sup>M. G. Moharam and T. K. Gaylord, *J. Opt. Soc. Am. A* **3**, 1780 (1986).

<sup>42</sup>M. G. Moharam, D. A. Pommet, E. B. Grann, and T. K. Gaylord, *J. Opt. Soc. Am. A* **12**, 1077 (1995).

<sup>43</sup>H. A. Macleod, *Thin-Film Optical Filters*, 3rd ed. (Institute of Physics, Bristol, 2001), p. 40.

<sup>44</sup>M. A. Green and M. Keevers, *Prog. Photovoltaics* **3**, 189 (1995).